Published June 27, 2011

THE JOURNAL OF CELL BIOLOGY

Cohesin, condensin, and the intramolecular centromere loop together generate the mitotic chromatin spring

Andrew D. Stephens,[1] Julian Haase,[1] Leandra Vicci,[2] Russell M. Taylor II,[2] and Kerry Bloom[1]

[1]Department of Biology and [2]Department of Computer Science, University of North Carolina at Chapel Hill, Chapel Hill, NC 27599

Sister chromatid cohesion provides the mechanistic basis, together with spindle microtubules, for generating tension between bioriented chromosomes in metaphase. Pericentric chromatin forms an intramolecular loop that protrudes bidirectionally from the sister chromatid axis. The centromere lies on the surface of the chromosome at the apex of each loop. The cohesin and condensin structural maintenance of chromosomes (SMC) protein complexes are concentrated within the pericentric chromatin, but whether they contribute to tension-generating mechanisms is not known. To understand how pericentric chromatin is packaged and resists tension, we map the position of cohesin (SMC3), condensin (SMC4), and pericentric LacO arrays within the spindle. Condensin lies proximal to the spindle axis and is responsible for axial compaction of pericentric chromatin. Cohesin is radially displaced from the spindle axis and confines pericentric chromatin. Pericentric cohesin and condensin contribute to spindle length regulation and dynamics in metaphase. Together with the intramolecular centromere loop, these SMC complexes constitute a molecular spring that balances spindle microtubule force in metaphase.

Downloaded from jcb.rupress.org on December 22, 2011

Introduction

Metaphase is the crucial stage in mitosis when condensed sister chromatids are tethered by cohesin and bioriented along the mitotic spindle in preparation for chromosome segregation. The fidelity of chromosome segregation involves the balance of the microtubule-based outward force with chromatin-based inward force. Each chromosome is attached to the spindle microtubules via the kinetochore, a specialized protein–DNA structure built at the centromere (Bouck et al., 2008; Cheeseman and Desai, 2008). Upon attachment of sister kinetochores to the mitotic apparatus, tension is generated between sister chromatids and consequently the pericentromere chromatin (Goshima and Yanagida, 2000; Tanaka et al., 2000; Pearson et al., 2001). Chromatin provides an inward force opposing the outward-directed microtubule force (Bloom and Joglekar, 2010). However, the molecular basis of this chromatin inward force has not been well characterized.

In budding yeast, the streamlined mitotic spindle provides an ideal model for biophysical studies. There are a limited number of microtubules (16 kinetochore microtubules and 4 interpolar microtubules from each pole and 40 microtubules per spindle; Winey et al., 1995). The centromeres are defined by DNA sequence (Fitzgerald-Hayes et al., 1982), and the 32 centromeres from 16 replicated chromosomes cluster into two foci upon biorientation in metaphase (Goshima and Yanagida, 2000; Pearson et al., 2004). Interpolar microtubules serve as tracks along which motor proteins move and act as struts to stabilize the bipolar spindle. The major function of microtubule motors within the spindle is to slide antiparallel microtubules apart, generating an outward spindle elongation force (Saunders and Hoyt, 1992). The pericentric chromatin opposes the action of the microtubule-based motor proteins (Bouck and Bloom, 2007). The decompaction of chromatin upon reduction of one of the core histones (H3) leads to increased metaphase spindle length. The increase in spindle length is suppressed by the loss of a microtubule-based motor protein, Kip1 or Cin8. The finding that pericentric chromatin length responds to the concentration of motor proteins led to the hypothesis that chromatin is an elastic spring.

The simplest form of an elastic spring is a Hookean spring in which applied force leads to a linear increase in length

Correspondence to Kerry Bloom: kerry_bloom@unc.edu

Abbreviations used in this paper: SMC, structural maintenance of chromosomes; WLC, wormlike chain; WT, wild type.

© 2011 Stephens et al. This article is distributed under the terms of an Attribution–Noncommercial–Share Alike–No Mirror Sites license for the first six months after the publication date (see http://www.rupress.org/terms). After six months it is available under a Creative Commons License (Attribution–Noncommercial–Share Alike 3.0 Unported license, as described at http://creativecommons.org/licenses/by-nc-sa/3.0/).

Supplemental Material can be found at:
http://jcb.rupress.org/content/suppl/2011/06/23/jcb.201103138.DC1.html

The Rockefeller University Press $30.00
J. Cell Biol. Vol. 193 No. 7 1167–1180
www.jcb.org/cgi/doi/10.1083/jcb.201103138

Published June 27, 2011

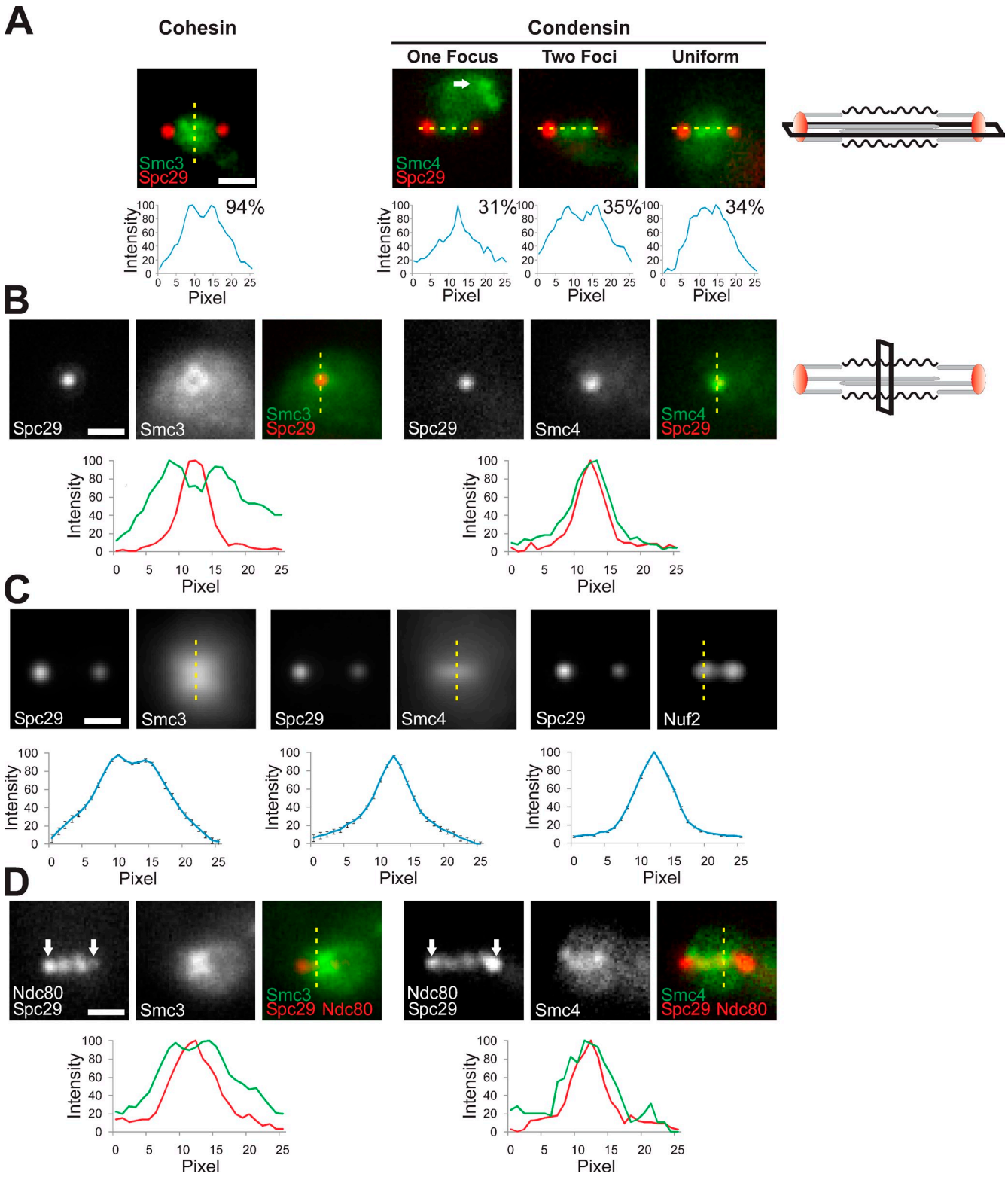

Figure 1. **Localization of cohesin and condensin in the pericentric chromatin.** (A) Smc3-GFP (cohesin) and Smc4-GFP (condensin) are enriched in the metaphase spindle between spindle pole bodies (Spc29-RFP). A line scan (dotted yellow line) of Smc3-GFP perpendicular to the spindle axis shows that cohesin has a bilobed enrichment. Line scans of Smc4-GFP taken along the spindle axis and between spindle pole bodies revealed three distinct classes of pericentric condensin enrichment: one focus, two foci, and uniform distribution left to right (n = 80, with percentages listed). Condensin ribosomal DNA localization is labeled with a white arrow. (B) Transverse (end on) images of Smc3-GFP display an area of low fluorescence and are displaced from the spindle pole. Smc4-GFP displays a diffraction-limited spot in line with the spindle pole body. Vertical line scans are shown as graphs below their respective images. (A and B) The schematics depict the image viewing angle of the mitotic spindle. In A, the spindle is viewed from the side/sagittal with both spindle poles in focus. In B, the spindle is viewed end on/transverse, and the spindle poles are aligned on top of each other so that only one pole is visible. (C) Ensemble-averaged images of Smc3-GFP, Smc4-GFP, and Nuf2-GFP (kinetochore protein) were generated by aligning and scaling multiple single-plane

Downloaded from jcb.rupress.org on December 22, 2011

Published June 27, 2011

(see Fig. 4 A). As chromatin is composed of approximately equal-weight DNA and protein, the physical properties of both are likely to contribute to properties of the spring. DNA behaves as a charged polymer that adopts a random coil conformation in vitro. The random coil reflects the tendency of individual monomeric units within the polymer to adopt a conformation with the greatest number of available states (i.e., greatest entropy). A model that describes this behavior is a wormlike chain (WLC; see Fig. 4 A; Bustamante et al., 1994; Peters and Maher, 2010). At low force regimes, small changes in force result in large length changes, as entropic force is exceedingly small. At high force regimes, in which the polymer approaches its full contour length (~90%), large changes in force result in small changes in length because of the large force it takes to stretch covalent bonds. To understand how tension is distributed between sister chromatids and how the tension-sensing spindle checkpoint functions, it is critical to determine whether chromatin springs behave with Hookean or WLC properties or both.

Micromanipulation of mitotic chromosomes reveals that their elasticity is dictated by both DNA and protein components. The major classes of nonhistone proteins that are likely to contribute to mitotic chromatin elasticity are topoisomerases, cohesin, and condensin (Almagro et al., 2004; Kawamura et al., 2010). Cohesin's main function is to hold together sister chromatid strands, whereas condensin's main function is to condense chromatin (Hirano, 2006; Nasmyth and Haering, 2009). Both cohesin and condensin are enriched in the pericentric chromatin by chromatin immunoprecipitation (Megee et al., 1999; Tanaka et al., 1999; Glynn et al., 2004; Weber et al., 2004; D'Ambrosio et al., 2008; Hu et al., 2011). The perturbation of pericentric cohesin or condensin results in the loss of proper tension sensing and error correction in metaphase (Yong-Gonzalez et al., 2007; Ng et al., 2009). Depletion of condensin leads to increased centromere stretching and dynamics in mammalian cells. This may indicate a role for a rigid spring in controlling chromosome dynamics and constant tension at the centromere (Ribeiro et al., 2009; Samoshkin et al., 2009; Uchida et al., 2009). Furthermore, cohesin has been demonstrated to set up kinetochore geometry (Sakuno et al., 2009), and experiments in *Caenorhabditis elegans* reveal that condensin is required for centromere resolution (Moore et al., 2005). Therefore, cohesin and condensin contribute to the architecture and elastic properties of the pericentric chromatin.

In this study, we have used digital microscopy and live cell dynamics to deduce the spatial distribution of cohesin, condensin, and DNA within the pericentric chromatin. Pericentric condensin is proximal to the spindle axis, whereas pericentric cohesin is distal to the mitotic spindle axis. Analysis of spindle and pericentric chromatin dynamics in cohesin and condensin mutants reveals that the intramolecular loop of pericentric chromatin, cohesin, and condensin behaves as a molecular spring with WLC properties in vivo.

Results

Pericentric cohesin and condensin are spatially segregated

Cohesin and condensin are enriched in the pericentric region but exhibit distinct patterns of localization. Cohesin (Smc3) exhibits a bilobed structure when viewed from the side (sagittal section of spindle; Fig. 1 A; Yeh et al., 2008). In contrast, condensin (Smc4) is enriched along the spindle axis as well as the nucleolus (Fig. 1 A, white arrow). The fraction of Smc4-GFP between the spindle poles is heterogeneous and appears either as a single focus, two foci, or a uniform distribution bounded by the spindle poles. These patterns occur in approximately equal frequencies ($n = 80$; Fig. 1 A). Thus, cohesin and condensin are differentially localized in the metaphase spindle (Bachellier-Bassi et al., 2008).

We used line scan data from single cells (Fig. 1, A and B) and ensemble-averaged images (Fig. 1 C) of cohesin and condensin to deduce the structures containing these protein complexes. Single-plane images taken with both spindle pole bodies in focus (sagittal section) were aligned horizontally. Each image was individually scanned along the x and y axis through the brightest pixel to obtain the mean distribution of Smc3 and Smc4 in the metaphase spindle. All single-cell images were then compiled into an ensemble-averaged image (Fig. 1 C). Line scans of the Smc3-GFP cohesin barrel yielded a peak-to-peak width of 373 ± 63 nm and a length of 560 ± 118 nm ($n = 34$; Fig. 1 C). Transverse (end on) images of cohesin display an area of low fluorescence signal and yielded a peak-to-peak measurement of 475 ± 62 nm ($n = 22$; Fig. 1 B). Condensin is proximal to the spindle axis and shows no bilobed structure in sagittal images. In transverse images, condensin appears as a single focus with no resolvable area of reduced fluorescence (Fig. 1 B). Line scans of single-plane Smc4-GFP sagittal images yielded a single peak with a Gaussian distribution 303 ± 51 nm wide (full width and half-maximum; Fig. 1 C) and 636 ± 198 nm in length ($n = 51$). Ensemble-averaged images and line scan analysis reveal that cohesin and condensin occupy two separate subdomains within the pericentric chromatin.

To position pericentric cohesin and condensin relative to known structures in the spindle, we analyzed the kinetochore proteins Nuf2 and Ndc80. Nuf2-GFP and Ndc80-GFP appear as two distinct foci, marking the plus ends of kinetochore microtubules (Goshima and Yanagida, 2000; Pearson et al., 2004). Kinetochore microtubules emanate from the spindle pole body and lie within an ~250-nm diameter around the spindle pole bodies (Winey et al., 1995; Gardner et al., 2005). Line scans of Nuf2-GFP and Ndc80-GFP yielded a Gaussian distribution of 291 ± 14 and 288 ± 11 nm, respectively (full width and half-maximum, $n = 21$ and 24; Fig. 1 C). Line scans of condensin have the same peak position along the spindle axis as kinetochores (Fig. 1 D). These data reveal that

images of each protein. Line scans of single-plane images were averaged and graphed to quantify the distribution. The error bars represent SEM (Smc3, $n = 34$; Smc4, $n = 51$; Nuf2, $n = 30$). (D) Images of Smc3 and Smc4 relative to the kinetochore (Ndc80) and spindle poles (Spc29; white arrows). Line scans are shown as graphs below their respective image. All line scan graphs display the relative fluorescence intensity plotted versus the distance in pixels (65 nm/pixel). Bars, 1 μm.

Downloaded from jcb.rupress.org on December 22, 2011

Published June 27, 2011

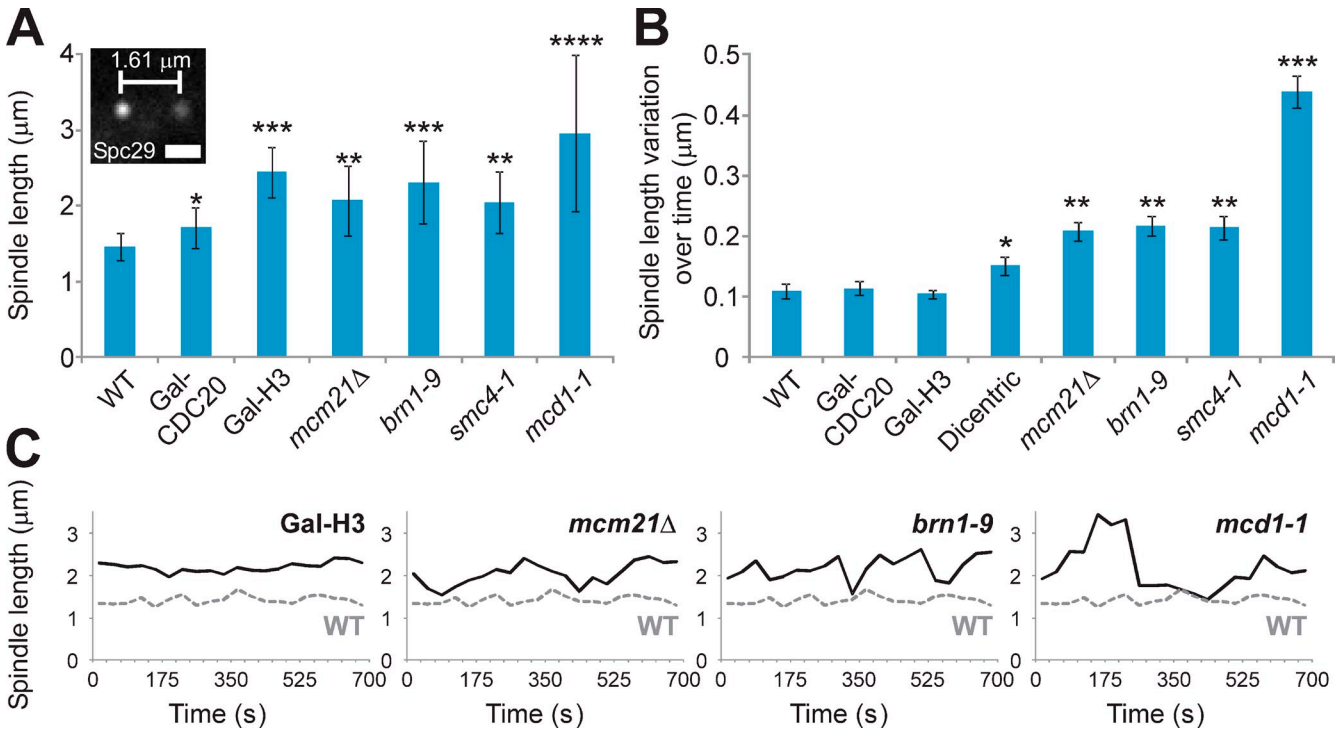

Figure 2. **Spindle length and variation increase upon depletion of cohesin and condensin.** (A) Spindle length was measured between the spindle pole bodies (Spc29-RFP) in metaphase cells of WT, Gal-CDC20, Gal-H3, cohesin mutants *mcm21Δ* and *mcd1-1*, and condensin mutants *brn1-9* and *smc4-1*. Cells were followed over time to ensure that measurements were taken in metaphase and not in linearly increasing anaphase spindles. The micrograph depicts a WT metaphase spindle. The white bracket represents spindle length as measured by the distance between the two spindle pole bodies. The error bars represent SEM. Bar, 1 µm. (B) Spindle length variation over time in metaphase is graphed for WT, Gal-CDC20, Gal-H3, cohesin mutants *mcm21Δ* and *mcd1-1*, condensin mutants *brn1-9* and *smc4-1*, and cells containing an active dicentric chromosome. Spindle pole bodies were filmed at 35-s intervals for 11.7 min. Variation in spindle length was calculated by the absolute value of the difference between spindle length at each time point and the mean spindle length over a time lapse. The error bars represent 95% confidence. (A and B) Mutants that are statistically significantly different ($P < 0.05$) from WT are marked with an asterisk. Mutants with the same number of asterisks are statistically similar ($P > 0.05$), whereas those with a different number of asterisks are statistically different ($P < 0.05$). (C) Representative graphs of spindle length over time for Gal-H3, *mcm21Δ*, *brn1-9*, and *mcd1-1* (black lines). WT is graphed (dashed gray lines) for comparison.

condensin resides along the spindle axis between the sister kinetochores. In contrast, line scans of cohesin reveal two peaks surrounding the spindle axis (Fig. 1 D). Pericentric cohesin is radially displaced from pericentric condensin and the spindle microtubules.

Cohesin and condensin contribute to metaphase spindle length and dynamics

To determine whether structural maintenance of chromosomes (SMC) protein complexes contribute to the physical properties of the spindle, we examined spindle dynamics in mutants that disrupt the organization of pericentric chromatin. We used temperature-sensitive alleles of cohesin *mcd1-1* (Guacci et al., 1997; Michaelis et al., 1997) and condensin *brn1-9* and *smc4-1* (Lavoie et al., 2000; Bachellier-Bassi et al., 2008) as well as deletion of the nonessential kinetochore protein Mcm21. Mcm21 is required for enrichment of pericentric cohesin, leaving arm cohesin and pericentric condensin unimpaired (Fig. S1; Eckert et al., 2007; Ng et al., 2009). To examine spindle length, we introduced markers for spindle pole bodies and measured the distance between them in metaphase. Metaphase spindles were defined by the presence of separated kinetochores >200 nm from the spindle poles and by the lack of persistent elongation (over a 12-min period). Wild-type (WT) spindle lengths were on average 1.46 ± 0.18 µm ($n = 54$; Fig. 2 A). *mcd1-1* mutants at restrictive temperature displayed the largest increase in spindle length to 2.96 ± 1.03 µm ($n = 50$). Reduction of cohesin from the pericentric chromatin in *mcm21Δ* cells resulted in a mean spindle length increase to 2.07 ± 0.46 µm ($n = 72$). Condensin mutants *brn1-9* and *smc4-1* at restrictive temperatures displayed an increase in spindle length to 2.3 ± 0.4 µm ($n = 80$) and 2.04 ± 0.55 µm ($n = 19$), respectively. In comparison, repression of H3 histones (Gal-H3), which decreases nucleosome occupancy to ~50% (Bouck and Bloom, 2007), resulted in a mean spindle length of 2.45 ± 0.34 µm ($n = 41$). Cells arrested in metaphase by Gal-CDC20 repression (Hartwell et al., 1973) displayed a small increase in spindle length (1.72 ± 0.27 µm, $n = 52$) but significantly less than that observed in the mutants. Therefore, cohesin, condensin, and nucleosomes contribute to spindle length regulation.

To reveal whether the increase in spindle length upon depletion of histones, cohesin, or condensin altered spindle length stability, we analyzed spindle length variation over time. Variation in spindle length was calculated by the absolute value of the difference between spindle length at each time point and the mean spindle length over a 12-min live single-cell time lapse. Variation represents the SD of all single time points across multiple cells. In WT cells, the spindle

Downloaded from jcb.rupress.org on December 22, 2011

Published June 27, 2011

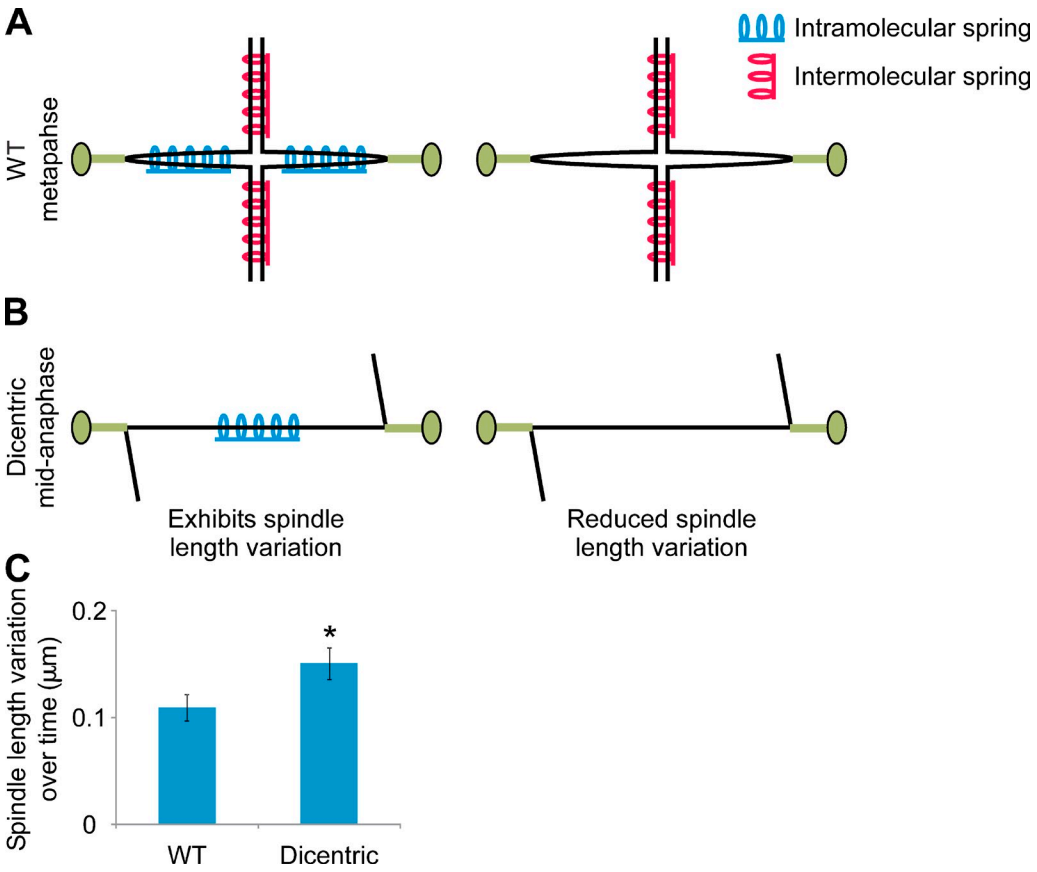

Figure 3. **Intra- and intermolecular chromatin springs.** (A) A bioriented sister chromatid pair under tension in metaphase is shown as containing both intramolecular springs (pericentromere loop in blue) and intermolecular springs (sister cohesion in red; left) or only intermolecular springs (right). (B) A mid-anaphase spindle with a dicentric chromosome bridge. Cohesin is cleaved, and monocentric chromosomes move to the spindle poles. The two centromeres on the same chromatid attach to opposite spindle poles, thereby creating a double-stranded DNA chromosome bridge. Cell cycle progression is delayed in mid-anaphase for ~45 min (Yang et al., 1997). (C) Variation in spindle length is graphed for WT and the active dicentric (data replotted from Fig. 2 B). The asterisk denotes that they are statistically different ($P < 0.05$). The error bars represent 95% confidence.

achieved a length of 1.46 µm with a mean variation in length of 109 nm (n = 180; Fig. 2 B). Upon histone repression, the spindle increased in length but exhibited variation comparable in magnitude with that of WT (Gal-H3: 105 nm, n = 740; Fig. 2, B and C). This indicates that variation is not a consequence of increased spindle length. Likewise, cells arrested in metaphase (Gal-CDC20) had similar spindle length variation to that of WT metaphase cells (114 nm, n = 321), suggesting that spindle length variation is not a consequence of metaphase arrest/delay.

Depletion of pericentric cohesin (*mcm21Δ*) or pericentric and arm cohesin (*mcd1-1*) resulted in a significant increase in spindle length variation (*mcm21Δ*: 208 nm, n = 600; *mcd1-1*: 439 nm, n = 859). Likewise, increased variation was observed upon depletion of condensin (*brn1-9*: 217 nm, n = 541; *smc4-1*: 214 nm, n = 706; Fig. 2, B and C). The increased length variation results from the changing distance between kinetochores and not from kinetochore microtubule length (Fig. S2 B). These data indicate that changes in chromatin length, and not kinetochore microtubules, are the source of spindle length fluctuations. Furthermore, cohesin and condensin are necessary to maintain a steady-state spindle length and thus serve a different mechanical function from that of nucleosomes.

Intra- versus intermolecular cohesin function

The predominant function of cohesin in metaphase is to hold sister chromatids together. To distinguish the contribution to spindle dynamics of intermolecular cohesin function from the intramolecular centromere DNA loop, we have used a dicentric chromosome in which cells initiate anaphase but delay cell cycle progression in midanaphase with a single dicentric chromosome bridge (Fig. 3 B; Yang et al., 1997). Midanaphase is defined by kinetochore-to-pole movement, shortening of kinetochore microtubules, and spindle elongation (Yang et al., 1997; Gardner et al., 2008). Pericentric cohesin is destroyed within 3–5 min of anaphase onset (Yeh et al., 2008). If spindle dynamics require intermolecular sister chromatid cohesion, spindle length variation will be reduced (Fig. 3, A and B, right). In contrast, if intramolecular force contributes to spindle dynamics, the midanaphase spindle will exhibit length variation (Fig. 3, A and B, left). There was a significant increase in spindle length variation to 151 nm (n = 303; from 109 nm in WT) but less than that observed with the loss of pericentric cohesin (*mcm21Δ*, 208 nm) or condensin (*brn1-9*, 217 nm; Figs. 2 B and 3 C). Condensin could be contributing to the intramolecular chromatin spring properties because its function is independent of cohesin in

Downloaded from jcb.rupress.org on December 22, 2011

Published June 27, 2011

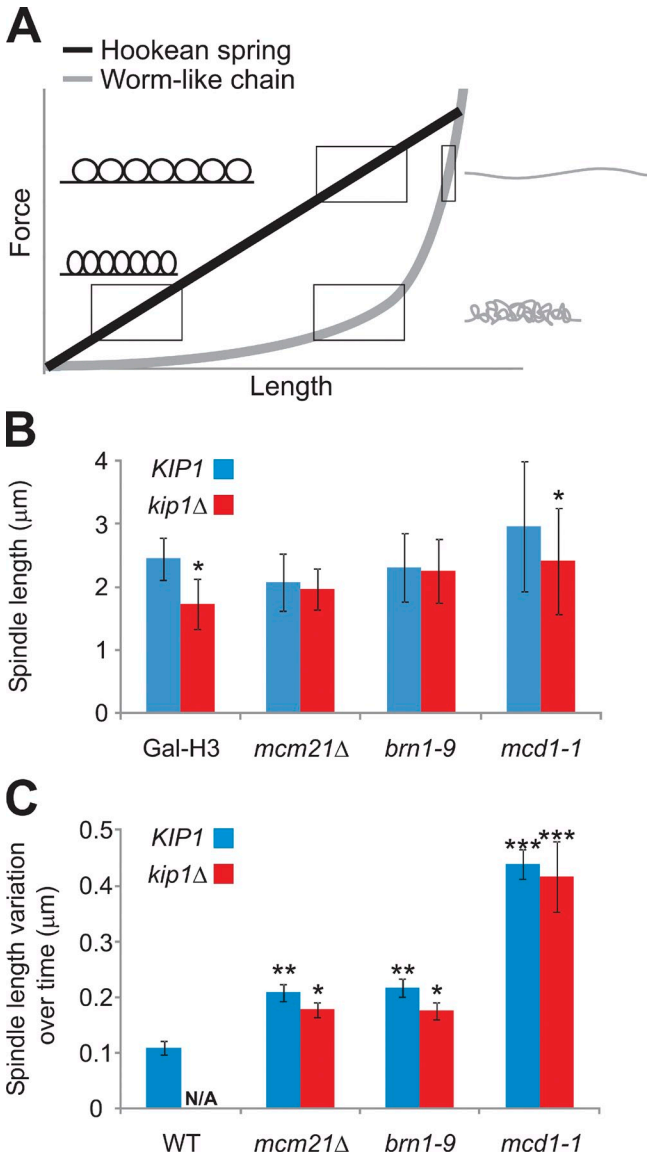

Figure 4. **Depletion of cohesin or condensin alters the elastic response of pericentric chromatin in cells deleted of *KIP1*.** (A) A Hookean spring has a linear force versus the extension curve in which the force applied is proportional to length ($F = -k(x-x_0)$, where F = force, k = spring constant, x_0 = rest length, and x = extended length). The circles to the left of the force extension curve denote the structure of the spring at different values of force. A WLC has an exponential force versus extension curve of $F = (k_BT/P)\,[1/4(1 - x/L)^{-2} - 1/4 + x/L]$, where F = force, k_B = Boltzmann constant, T = temperature, P = persistence length, L = contour length, and x = extended length. Gray lines to the right of the force extension curve denote the structure of the WLC at low force (random coil) and an extended chain (wavy line) at higher force. Large rectangles denote linear force versus extension, whereas the slim rectangle denotes nonlinear portions. (B) Metaphase spindle length was measured between the spindle pole bodies (Spc29-RFP) in Gal-H3, *mcm21Δ*, *brn1-9*, and *mcd1-1* single mutants with *KIP1* and double mutants with *kip1Δ*. The error bars represent SD. Statistically different ($P < 0.05$) *KIP1* versus *kip1Δ* spindle lengths are marked by an asterisk. (C) Spindle length variation was measured by tracking the spindle pole bodies every 35 s for 11.7 min in Gal-H3, *mcm21Δ*, *brn1-9*, and *mcd1-1* single mutants with *KIP1* and double mutants with *kip1Δ*. The error bars represent 95% confidence. Spindle length variation that is statistically different ($P < 0.05$) from that of WT is marked with an asterisk. Mutants with the same number of asterisks are statistically similar ($P > 0.05$), whereas those with a different number of asterisks are statistically different ($P < 0.05$).

anaphase (Lavoie et al., 2004). The elastic properties of chromatin are evident in a single chromosome bridge, and, therefore, the chromatin spring does not require intermolecular cohesion between sister chromatids.

Physical properties of the intramolecular chromatin spring

To determine the physical properties of the chromatin spring, we introduced a mutation to reduce the magnitude of the outward-directed, microtubule-based spindle force (Saunders and Hoyt, 1992; Straight et al., 1998). If pericentric chromatin behaves as a simple Hookean spring, decreasing the outward force should cause the chromatin spring to recoil and decrease spindle length (Fig. 4 A, black line). Alternatively, if the spring has WLC properties, recoil is not linearly related to force (Fig. 4 A, gray line). Upon deletion of the microtubule-based motor protein Kip1, spindles in WT (Saunders and Hoyt, 1992; Straight et al., 1998) and cells with reduced nucleosome occupancy (Bouck and Bloom, 2007) display an elastic response (Fig. 4 B). In contrast, *mcm21Δ;kip1Δ* and *brn1-9;kip1Δ* double mutant cells showed no significant change in spindle length (*mcm21Δ*: 1.97 ± 0.33 μm, $n = 70$; *brn1-9*: 2.26 ± 0.51 μm, $n = 74$; Fig. 4 B). Spindle length in *mcd1-1;kip1Δ* was reduced from 2.96 ± 1.03 to 2.42 ± 0.84 μm ($n = 60$) but not to the same extent as histone repression. Likewise, variation in spindle length was not rescued upon deletion of *KIP1* (Fig. 4 C). Spindles lacking pericentric cohesin or condensin do not recoil as predicted for a simple Hookean spring (Fig. 4, A and B). Either pericentric cohesin or condensin acts as a spring in the spindle, or the pericentric chromatin behaves as a WLC approaching its full extension upon loss of cohesin or condensin (Fig. 4, A and B).

Spring length versus extension

The increase in spindle length could arise from an increase in chromatin spring length or the degree of chromatin extension. To distinguish between these possibilities, we examined the compaction of pericentric LacO arrays in WT and mutant cells. In WT cells, pericentric-linked LacO arrays are dynamic and transiently separated in metaphase (Fig. 5 A, WT; Goshima and Yanagida, 2000; Tanaka et al., 2000; Pearson et al., 2001). LacO arrays appear as spots or filaments indicative of chromatin decompaction and stretching (Fig. 5 A; Bachant et al., 2002; Warsi et al., 2008). Stretching of a LacO array 6.8 kb from the centromere occurs in ~10% of WT cells ($n = 167$). Upon histone repression, LacO spot dynamics are indistinguishable from WT ($n = 89$; Fig. 5 A; Bouck and Bloom, 2007). In contrast, stretching of the pericentric LacO arrays was observed in >50% of cells depleted of pericentric cohesin or condensin (*mcm21Δ*, $n = 83$; *brn1-9*, $n = 106$; Fig. 5 A). In these cells, the occurrence of stretched pericentric LacO spots was positively correlated with longer spindles (Fig. 5 B). Time-lapse analysis of pericentric LacO in *mcm21Δ* and *brn1-9* cells revealed multiple stretching, and recoil events occur with a time constant similar to that of spindle growth and shortening (Fig. S3). The increased frequency of stretching reveals that the LacO arrays are more likely to adopt a linear conformation in the absence of condensin or cohesin. In contrast, the lack of stretching upon

Downloaded from jcb.rupress.org on December 22, 2011

Published June 27, 2011

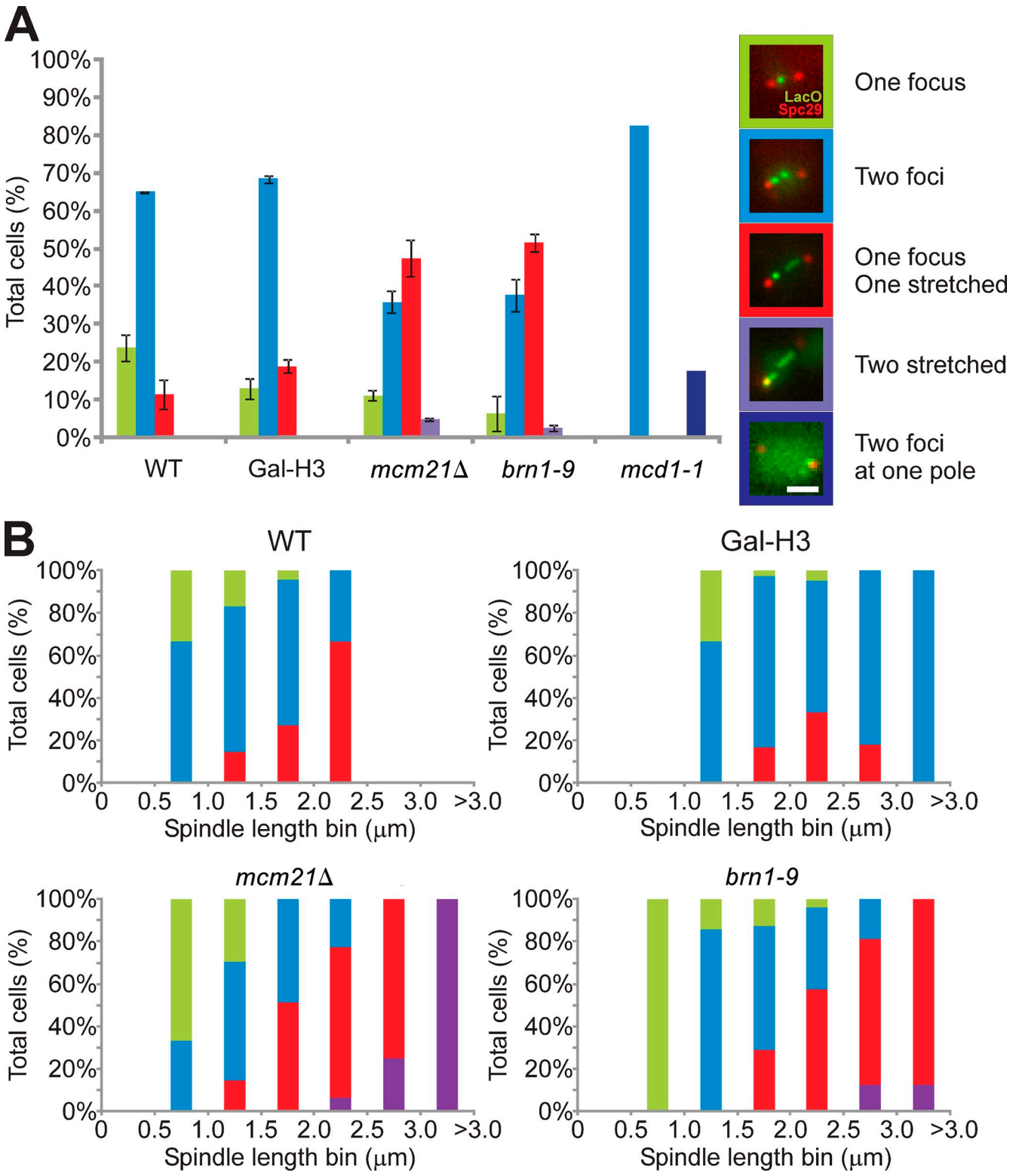

Figure 5. **Increased stretching of pericentric chromatin LacO spots in pericentric cohesin and condensin mutants.** (A) Pericentric LacO 6.8 kb from CEN 15 images were classified as one focus, two foci, one focus and one stretched, two stretched, and two foci at one pole. The percentages of cells displaying each class of LacO fluorescence for each strain background are graphed with representative images of each class to the right (WT: 24 ± 4% single focus, 65 ± 0% two foci, 11 ± 4% one stretched, three experiments, n = 167; Gal-H3: 13 ± 3% single focus, 68 ± 1% two foci, 19 ± 2% one stretched, two experiments, n = 89; *mcm21Δ*: 11 ± 1% single focus, 36 ± 3% two foci, 47 ± 5% one stretched, 5 ± 0% two stretched, two experiments, n = 106; *brn1-9*: 6 ± 5% single focus, 38 ± 2% two foci, 52 ± 2% one stretched, 3 ± 1% two stretched, two experiments, n = 83; *mcd1-1*: 82% two foci, 18% two foci at one pole, one experiment, n = 17). The error bars represent SD. Bar, 2 μm. (B) The percentage of total cells compiled from all experiments displaying each class of LacO fluorescence is binned by spindle length into bins of 0.5 μm and graphed for WT, Gal-H3, *mcm21Δ*, and *brn1-9*. The data are the same for those described in A. Means and SEM values are listed in Table S1.

Downloaded from jcb.rupress.org on December 22, 2011

Published June 27, 2011

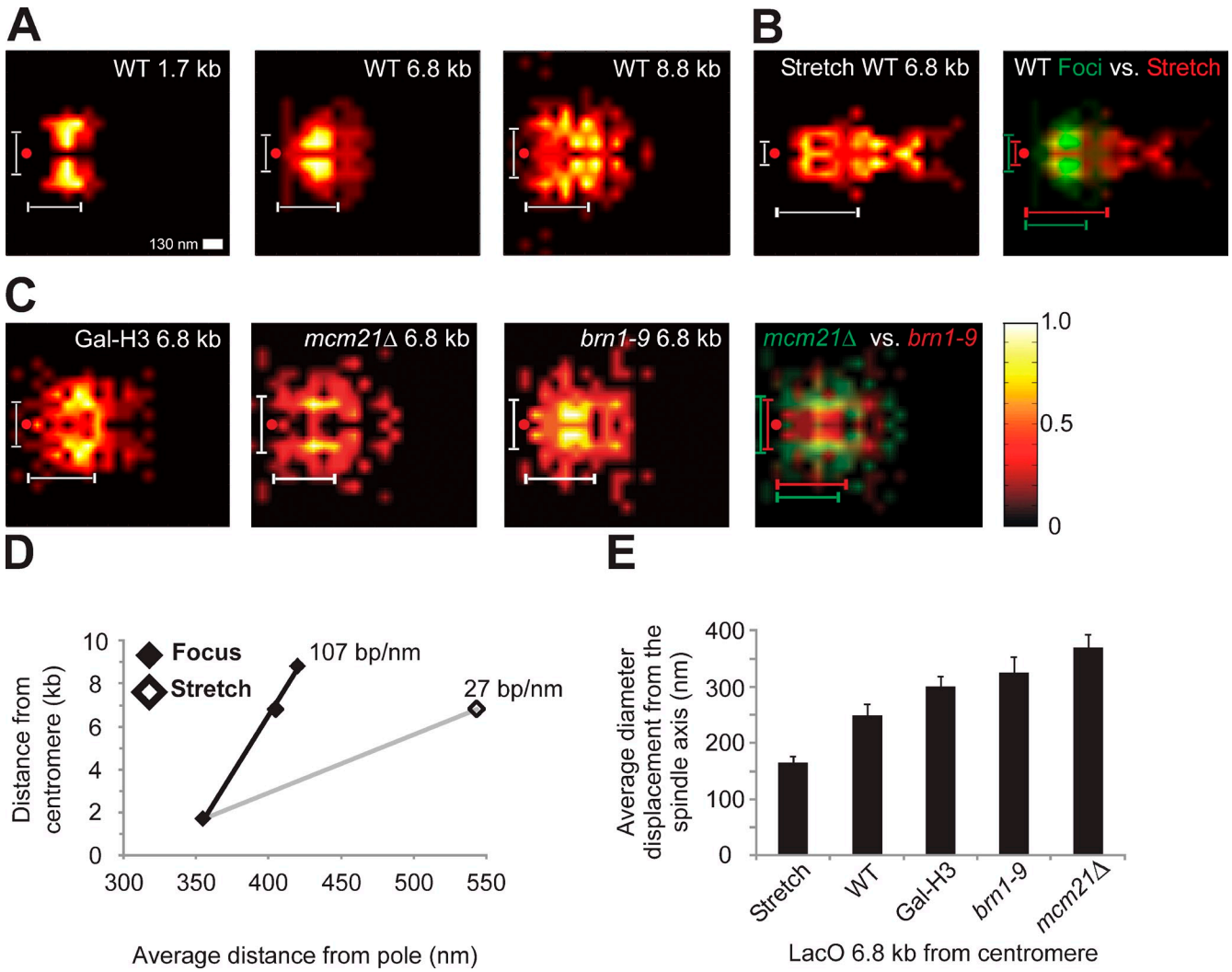

Figure 6. **Density maps of pericentric LacO show differences in the position probability.** (A) The mean position of WT pericentric LacO 1.7 kb from CEN 3, LacO 6.8 kb from CEN 15, and 8.8 kb from CEN 3 was determined in metaphase spindles by mapping the peak intensity of the LacO relative to the spindle pole body (red circles). The number and position of peak LacO intensity were used to generate a color-coded heat map of pericentric chromatin position in the spindle. (B) Position probability of WT pericentric LacO 6.8 kb displaying a stretched line signal. An overlay of WT 6.8 kb foci (green) and WT 6.8 kb stretching (red) heat maps allows for comparison. (C) Position probability of pericentric LacO 6.8 kb is altered distinctly in Gal-H3, *mcm21Δ*, and *brn1-9*. An overlay of *mcm21Δ* (green) and *brn1-9* (red) heat maps allows for comparison. (A–C) Vertical white brackets represent mean diameter, and horizontal white brackets represent the mean distance from the spindle pole (values in Table I). (D) Graph of LacO distance from centromere in base pairs versus the distance from the pole in nanometers (WT LacO, 1.7, 6.8, and 8.8 kb [◆, black line]; and WT stretched, 6.8 kb [◇, gray line]). (E) A bar graph of mean diameter displacement perpendicular to the spindle axis for the LacO array 6.8 kb from the centromere in stretched, WT, Gal-H3, *brn1-9*, and *mcm21Δ*. The error bars represent SEM. The data and number of experiments for D and E are summarized in Table I.

histone depletion reveals that the LacO arrays remain in their compact state. These data indicate that the pericentric chromatin spring approaches its full extent in the absence of pericentric cohesin or condensin and behaves as a WLC upon the reduction of outward force (Fig. 4).

Contribution of histone, cohesin, and condensin to the organization of pericentric chromatin

To determine how cohesin and condensin contribute to the organization of the pericentric chromatin, we mapped the distribution of pericentric LacO arrays in WT cells. LacO arrays were inserted at 1.1, 1.8, and 3.8 kb from the centromere. The centroid of the LacO array in these strains is 1.7, 6.8, and 8.8 kb from the centromere, respectively (see Materials and methods). Spatial probability maps were generated by taking the peak intensity of LacI-GFP bound to the LacO array and plotting the position relative to the spindle pole body (Spc29-RFP). The Cartesian coordinates (x and y) from multiple cells (1.7 kb, $n = 39$; 6.8 kb, $n = 81$; 8.8 kb, $n = 76$) were used to generate a heat map that represents the distribution of the pericentric LacO relative to the spindle pole (Fig. 6 A). Because the rotation of the spindle is random in individual cells, the Cartesian quadrant we obtain is actually one slice of the cylindrical arrangement of pericentric chromatin around the spindle. To illustrate the 3D geometry, we mirrored the heat map about the spindle axis as it would be viewed from a single plane through the middle of the spindle (Fig. 6 A).

Downloaded from jcb.rupress.org on December 22, 2011

Published June 27, 2011

Table I. **Mean position of centromere-proximal LacO spots in WT and chromatin mutants**

Type	*n*	Distance from spindle pole		Diameter around spindle axis		Percent proximal
		Mean	SD	Mean	SD	
		nm	*nm*	*nm*	*nm*	%
WT 1.7 kb	39	355	69	285	124	20
WT 6.8 kb	81	405	136	250	172	45
WT stretch 6.8 kb	87	544	262	165	115	62
WT 8.8 kb	76	420	175	326	220	34
Gal-H3 6.8 kb	95	445	186	300	177	30
mcm21Δ 6.8 kb	85	408	227	370	218	18
brn1-9 6.8 kb	72	455	185	325	237	39

Percent proximal, LacO centroids fall within a 130-nm diameter around the spindle axis.

LacO arrays 1.7 kb from the centromere exhibit a distribution of 285 ± 124 nm in diameter and 355 ± 69 nm from the spindle pole (n = 39; Fig. 6 A and Table I). The distance from the spindle pole body is consistent with the estimated length of kinetochore microtubules (350 nm) obtained from tomography and model convolution microscopy (Winey et al., 1995; Gardner et al., 2005). LacO arrays 6.8 kb from the centromere reside 250 ± 172 nm in diameter and 405 ± 136 nm from the spindle pole (n = 81; Fig. 6 A). LacO arrays at 8.8 kb from the centromere reside 326 ± 220 nm in diameter and 432 ± 175 nm from the spindle pole (n = 76; Fig. 6 A and Table I). 95% of all WT LacO arrays fall within a diameter of 520 nm around the spindle axis. The distance of the centroid of the LacO array in base pairs from the centromere versus the mean distance from the spindle pole is an estimate of the packing ratio (Fig. 6 D). The pericentric DNA (1.7–8.8 kb) is compacted a mean of 107 bp/nm (Fig. 6 D, black line) or fivefold greater than a nucleosome fiber (21 bp/nm).

If the LacO stretching is a mechanical response to increased force, the chromatin fiber would be expected to stretch along the spindle axis. Mapping the probability distribution of stretched 6.8 kb WT LacO revealed that stretched pericentric chromatin lies closer to the spindle axis (165 ± 115 nm) and further from the spindle pole body (544 ± 262 nm; n = 87; Fig. 6 B and Table I). Interestingly, the mean distance of the stretched 6.8 kb array relative to the position of the 1.7 kb array reveals that the packing ratio decreased from 107 to 27 bp/nm (Fig. 6 D, gray line). This is comparable with nucleosome chromatin compaction. The stretching events observed in WT cells confirm that the force along the spindle axis is mechanically opposed by cohesin and condensin and that stretched chromatin is a linearly extended nucleosome fiber.

Histone repression (Gal-H3) and the loss of condensin (*brn1-9*) resulted in a significant increase in the mean distance of the 6.8 kb LacO foci from the spindle pole, from 405 nm (WT) to 445 ± 186 nm (n = 95) and 455 ± 185 nm (n = 72; Fig. 6 C and Table I). This increase in length corresponds to a twofold decompaction compared with WT (53 vs. 107 bp/nm WT). This value is similar to the twofold compaction observed upon cell cycle progression from G1 to M phase (Guacci et al., 1994). The Gal-H3 6.8 kb LacO probability distribution map becomes broader as well (Fig. 6 C). The loss of pericentric cohesin (*mcm21Δ*) did not alter the mean distance of the 6.8 kb LacO foci from the spindle pole (408 ± 227 nm, n = 85). In contrast, the mean diameter of the pericentric chromatin that encircles the spindle increased from 250 nm (WT) to 370 ± 218 nm (*mcm21Δ*; Fig. 6, C and E; and Table I). In addition, there was a decrease in the distribution of LacO spots proximal to the spindle axis (Fig. 6 C and Table I). Histone and condensin compact the pericentric chromatin axially, whereas cohesin contributes to radial compaction. These data are consistent with the location of condensin along the spindle axis versus cohesin, which is radially displaced. Therefore, the distribution of cohesin and condensin reflects their distinct functional roles in organizing the pericentric chromatin.

Discussion

The SMC-containing complexes cohesin and condensin are responsible for chromosome pairing and condensation in mitosis. They are enriched in the pericentric region surrounding the centromere in metaphase and form a novel bipartite cylinder that encircles the spindle microtubules. This cylindrical arrangement of pericentric chromatin functions as a molecular spring that opposes the largely outward-directed, microtubule-based force.

The geometric arrangement of cohesin surrounding the spindle microtubules raises several questions. There are inconsistencies in the simple C-loop model (Fig. 7 A; Yeh et al., 2008) with the distribution of cohesin based on chromatin immunoprecipitation and the position of the cohesin barrel (Fig. 1). Loops of 40–50 kb organized into a canonical nucleosomal beads-on-a-string extend ~1,000–1,200 nm from the chromosome axis (Fig. 7 A). This length (1,200 × 2 = ~2,400 nm) is three times the distance between kinetochore microtubules from each spindle pole (~800 nm). Additionally, if the DNA loops extend linearly between kinetochore microtubule plus ends, fluorescence from cohesin and condensin should overlap with the mitotic spindle. In contrast, cohesin and condensin are largely nonoverlapping with cohesin radially displaced relative to the diameter of condensin and the kinetochores (Fig. 1).

We have considered two alternative models that are consistent with both the localization of cohesin and condensin and the position of centromere-linked LacO arrays. One model is that 40–50 kb of pericentric chromatin is organized into a 30-nm fiber (Fig. 7 B). Alternatively, the centromere DNA loop adopts a random coiled or branched conformation reminiscent of DNA loops

Downloaded from jcb.rupress.org on December 22, 2011

Published June 27, 2011

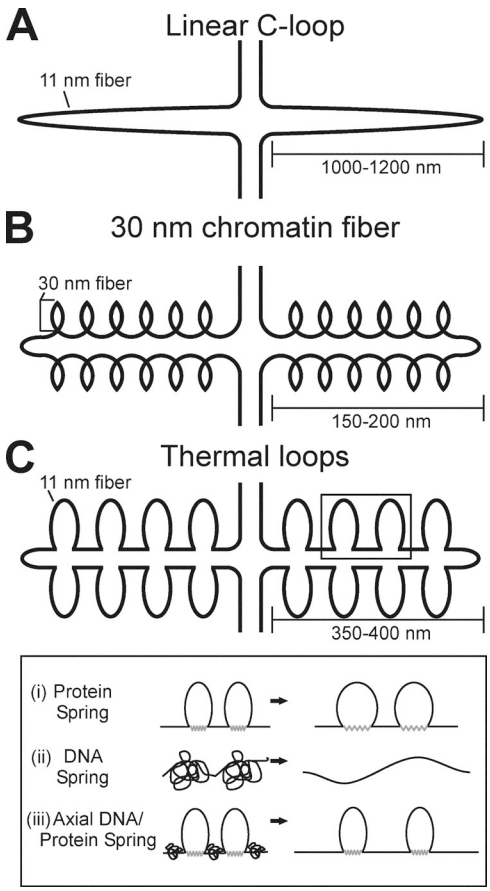

Figure 7. **Models of the pericentric chromatin spring.** (A–C) The pericentric chromatin (40–50 kb) is modeled as a linear loop (A), a 30-nm chromatin fiber (B), or a network of thermally fluctuating loops, denoted as thermal loops (C). The inset details three spring models: (i) the protein spring, in which cohesin and/or condensin (gray) linked via DNA are the elastic elements; (ii) the DNA spring, in which the DNA WLC adopts a random coil that expands and contracts in response to force; and (iii) the axial DNA/protein spring, in which protein springs limit the amount of DNA under tension, which in turn increases the spring constant. Elastic proteins and the DNA WLC expand and contract in response to force.

observed in regions of very active transcription such as the ribosomal DNA locus and mammalian kinetochores (Fig. 7 C; Bloom and Joglekar, 2010). In both models, thermal or active fluctuation of the fiber/loops could account for the observed radial displacement of DNA and cohesin. To estimate the packing ratio of pericentric chromatin, we mapped the position of centroids of LacO arrays at increasing distances from the centromere (Fig. 6). We found that the pericentric chromatin 1.7–8.8 kb has a packing ratio of 107 bp/nm, which is equivalent to the predicted packing ratio of a 30-nm fiber (Finch and Klug, 1976; Tremethick, 2007). If the pericentric chromatin is organized into a 30-nm fiber, the loss of nucleosomes would have a disproportional contribution to spindle length because there would be an ~45-nm increase in length for each lost nucleosome (50 nm of the b form − 5 nm of the nucleosomal). Because there is only a 50% increase in length observed upon histone repression, it is unlikely that 40–50 kb of the 30-nm chromatin fiber contributes to spindle length regulation. Likewise, the packing of the 30-nm fiber would not be expected to depend on cohesin and condensin, which is inconsistent with the increase in spindle length observed upon depletion of these complexes.

In the random or thermal loop model (Fig. 7 C), cohesin and condensin contribute to spindle length via their function in condensing or bridging loops. Condensin has been hypothesized to compact chromatin into loops (Kimura and Hirano, 1997; Yoshimura et al., 2002; Strick et al., 2004; Hirano, 2006), whereas cohesin may function to stabilize or bridge neighboring loops that are displaced from the spindle axis. Cohesin's looping function has recently emerged from studies on transcriptional regulation at a distance (Mishiro et al., 2009; Nativio et al., 2009; Guillou et al., 2010; Hou et al., 2010; Kagey et al., 2010). The tendency of cohesin to be displaced from the spindle may reflect its mobility after loading (Glynn et al., 2004; Lengronne et al., 2004; Hu et al., 2011). Alternatively, condensin may aid in displacing cohesin from the core centromere as it does in *C. elegans* to facilitate centromere resolution (Moore et al., 2005). The spatial distributions and/or functional interdependency between the two complexes may contribute to their similar effects on spindle length (Guacci et al., 1997; Lavoie et al., 2002, 2004; Lam et al., 2006; Heidinger-Pauli et al., 2010).

There are several different mechanisms in which the DNA and/or SMC complexes may contribute to the chromatin spring. First, condensin and/or cohesin are protein springs, and DNA provides a mechanism to link multiple condensins/cohesins in series (Fig. 7 C, i). Upon depletion of pericentric cohesin or condensin, there is a loss of chromatin elasticity, as indicated by increased pericentric LacO extension and spindle length variation. HEAT repeats that are present in the auxiliary subunits of SMC protein complexes (Neuwald and Hirano, 2000; Panizza et al., 2000) have been shown to be elastic elements that link force to catalysis in protein phosphatase PP2A (Grinthal et al., 2010). Second, the DNA WLC constitutes the spring (Fig. 7 C, ii). The WLC is a nonlinear entropic spring that reflects the tendency of a long-chain polymer to adopt a random coil. It takes very low force to significantly extend the random coil because the applied force is working against entropy. When the chain reaches ~90% of its overall length (contour length), the force extension curve increases exponentially as the applied force works against covalent bonds. In a WLC mechanism, we propose that nucleosome depletion results in an increase in overall spring length. The spring remains in the linear region of the WLC curve (Fig. 4), and chromatin recoils upon deletion of *KIP1*. Depletion of pericentric cohesin or condensin results in full extension of the WLC (pericentric LacO stretching; Fig. 5). In this realm of the force extension curve, changes in force have little effect on length (Fig. 4), consistent with the lack of recoil upon deletion of *KIP1*. A third mechanism is that condensin/cohesin protein springs limit the length of DNA under tension, thereby increasing the entropic DNA spring constant (Fig. 7 C, iii). The spring constant of a polymer-like DNA is inversely proportional to its chain length (Grosberg and Khokhlov, 1997); thus, restricting the length of DNA axially will increase the spring constant. The pericentric chromatin spring consists of elastic proteins as well as a long-chain DNA polymer. The spring exhibits properties of a Hookean spring or a WLC depending on the geometry and composition of proteins and the percentage of extension and/or overall length of the entropic DNA spring.

Downloaded from jcb.rupress.org on December 22, 2011

Published June 27, 2011

Spindle length fluctuation is a read-out of the stiffness of the chromatin spring. By mutation of one component, we can estimate a minimal spring constant from thermal fluctuations. Thermal fluctuations acting on an object are given by the equipartition theorem $\sigma^2 = k_BT/k$, where σ^2 = variation squared, k_BT = Boltzmann constant (4 pN·nm), and k = spring constant. Because other parameters are held constant (i.e., cells differ only in the mutation of interest), the equipartition theorem allows us to convert spindle length variation into an estimated spring constant. The spring constant was calculated using k_BT at 300° Kelvin divided by the experimentally measured spindle length variation squared (σ^2). The WT spring constant was calculated to be 0.345 pN/µm (k = 4.1 pN·nm/(109 nm)^2). Repression of nucleosomes increased spindle length but did not significantly alter spindle variation or spring constant (0.372 pN/µm Gal-H3 vs. 0.345 pN/µm WT). Therefore, histones dictate the rest or contour length of the chromatin spring rather than the spring constant. Interestingly, this calculated spring constant is comparable to the estimated force the anaphase spindle exerts on a single DNA molecule in living cells (0.2–0.42 pN/µm; Fisher et al., 2009).

Upon depletion of pericentric cohesin or condensin, the spring constant decreased to 25% of WT (0.095 pN/µm *mcm21Δ* and 0.087 pN/µm *brn1-9*). Thus, pericentric cohesin and condensin contribute to the spring constant of pericentric chromatin (intramolecular spring). The loss of pericentric and arm cohesin in *mcd1-1* mutants at a restrictive temperature decreased the spring constant to 6% (0.021 pN/µm) of WT, indicating that arm cohesion (intermolecular spring) contributes to the chromatin spring constant as well.

These data provide the first structural basis for chromatin springs in the spindle. The DNA packaging function of histones is translated into the spring length rather than spring constant. Condensin is concentrated along the spindle axis and contributes to the chromatin spring by resisting the outward force of the spindle. Cohesin contributes to the chromatin spring from a distal position. In addition, cohesin functions to confine and compress the pericentric chromatin to a position along the spindle axis. Human cells that are retinoblastoma protein depleted have decreased levels of pericentric cohesin and condensin and an increased pericentric chromatin length (Manning et al., 2010). The loss of checkpoint tension sensing reported in yeast pericentric cohesin, *mcm21Δ* (Ng et al., 2009), and condensin mutants (Yong-Gonzalez et al., 2007) underscores the importance of the chromatin spring. Mammalian cells depleted of condensin also show a decreased ability to properly sense tension at the kinetochore (Ribeiro et al., 2009; Samoshkin et al., 2009; Uchida et al., 2009). We propose that cohesin and condensin contribute to the structure and function of the pericentric chromatin spring that is conserved from yeast to higher eukaryotes to facilitate the faithful segregation of the genome in mitosis.

Materials and methods

Cell preparations

Cells were incubated in YPD (2% glucose, 2% peptone, and 1% yeast extract) at 32°C for WT strains. Temperature-sensitive strains containing *mcd1-1*, *brn1-9*, and *smc4-1* were grown at 24°C. Temperature-sensitive strains were grown into early log phase at 24°C and then shifted to restrictive temperature at 37°C for 3 h before filming. Temperature-sensitive stains were then viewed at RT for no longer than 45 min. Gal-H3 strains were α factor arrested in YPG (2% galactose), washed, and then released into YPD (2% glucose) for 3–4 h before viewing, as outlined in Bouck and Bloom (2007). Gal-CDC20 strains were grown into logarithmic phase in YPG, washed, and then grown in YPD for 3 h before imaging. Dicentric strains were grown in YPG to maintain a monocentric chromosome III to logarithmic phase, washed, and then grown in YPD to activate the dicentric for 1–2 h before imaging as outlined in Yang et al. (1997).

Microscopy

Wide-field microscope images were acquired at RT (25°C) using a microscope stand (Eclipse TE2000-U; Nikon) with a 100× Plan Apo 1.4 NA digital interference contrast oil emersion lens with a camera (Orca ER; Hamamatsu Photonics). MetaMorph 6.1 software (Molecular Devices) was used to acquire unbinned z series image stacks with a z step size of 300 nm. Imaging of Smc3/Smc4-GFP was performed in water on ConA-coated coverslips. Live imaging of cells was performed on a 25% gelatin slab with yeast complete 2% glucose media. Image exposure times were between 300 and 700 ms.

Analyzing Smc3 and Smc4 fluorescence

MATLAB (MathWorks, Inc.) was used to rotate the spindle axis of MetaMorph images horizontally using Spc29-RFP as markers of spindle ends. Horizontally rotated images could then be analyzed in MetaMorph with the brightest pixel of both spindle pole bodies along the same y coordinates. Line scans 1 pixel in width and length of the spindle were drawn along the spindle axis of images containing Smc4-GFP and Spc29-RFP in MetaMorph. The data of pixel position and intensity of Smc4-GFP were transferred to Excel (Microsoft) and graphed to determine the classification (one focus, two foci, or uniform signal) of condensin enrichment between the spindle poles.

Only single-plane images from z series acquisitions containing both Spc29-RFP spindle pole bodies in focus with metaphase length spindles of 1.3–1.7 µm were used for analyzing Smc3, Smc4, or Nuf2-GFP. Each single-plane image was rotated using MATLAB to align all spindles axes horizontally along the same y coordinate. Using MetaMorph, line scans of each single-plane image were taken perpendicular and parallel to the spindle axis and through the maximum pixel intensity. These line scans were averaged and graphed using Excel to show the mean distribution of both Smc3 and Smc4 perpendicular (width/diameter around the spindle axis) and parallel (length along the spindle axis) to the spindle axis. Smc3 width was measured by the inclusive pixel coordinates from peak to peak of the bilobed enrichment. Smc4 and Nuf2 width was measured in MATLAB by fitting a Gaussian distribution to the line scan through the brightest pixel to obtain a full-width, half-maximum measurement. Lengths of Smc3 and Smc4 enrichment were measured along the x axis by using the distance between the pixel coordinates at half-maximum above the nuclear background using MetaMorph.

Mean distribution pictures were generated using already rotated images of cohesin, condensin, or kinetochore proteins with spindle poles. Rotated images were then color combined (Spc29-RFP and Smc3/4-GFP of Nuf2-GFP) in MetaMorph and saved. The color-combined stacks were separated into single-plane, color-combined sequential images by ImageJ (National Institutes of Health). The sequential series of single-plane, color-combined pictures were loaded into Video Optimizer software (University of North Carolina at Chapel Hill) to be scaled to the mean spindle length and generated a mean Smc3, Smc4, and Nuf2-GFP fluorescence signal between spindle pole bodies.

Spindle length and variation

Spindle lengths were measured by logging the coordinates of the brightest pixel of each spindle pole body, marked by Spc29-RFP, using MetaMorph. Coordinates of pixel position were measured in triplicate. The coordinates of sister spindle poles were transferred to Excel and converted into distance spindle length in micrometers. Spindle lengths were measured in two dimensions and three dimensions using the Pythagorean theorem. Time-lapse videos were performed on single cells using Acquire Timelapse in MetaMorph to take a z series every 35 s for 20 time points, equaling 11.67 min. Change in spindle length, denoted as variation, was calculated by the absolute value of the difference between spindle length at each time point and the mean spindle length of the time lapse. All metaphase spindle lengths and time lapses were taken in spindles of at least 1.1 µm, with separated Nuf2 kinetochore foci and spindles not exhibiting linearly increasing anaphase spindle behavior.

Analyzing pericentric LacO array stretching and position

LacO/lacI-GFP strains were grown in SD-His media to induce lacI-GFP under the *HIS* promoter as outlined by Goshima and Yanagida (2000) and

Downloaded from jcb.rupress.org on December 22, 2011

Published June 27, 2011

Pearson et al. (2001). The centroids of the LacO arrays were 1.7 kb from CEN 3 in strain KBY 8088 (1.2-kb array inserted at 1.1 kb from CEN 3), 6.8 kb from CEN 15 in strain KBY 8065 (10-kb array inserted at 1.8 kb from CEN 15), and 8.8 kb from CEN 3 in strain KBY 8087 (10-kb array inserted at 3.8 kb from CEN 3). Images were captured using unbinned and 2 × 2 binning acquisitions and were analyzed in MetaMorph using line scans to determine focus versus stretching LacO spots. Focus LacO spots were determined by a Gaussian distribution line scan through the brightest pixel. Stretched LacO was determined by a non-Gaussian distribution or broadening of the line scan with an ~0.5 decrease in brightest pixel fluorescence signal compared with a focus.

2D density maps were generated of LacO/lacI-GFP spots relative to the spindle pole body (Spc29-RFP) as outlined in Anderson et al. (2009). Single-plane images were rotated using MATLAB to align all spindle axes horizontally along the same y coordinate. The distance in pixels from each LacO/lacI-GFP brightest pixel to its respective spindle pole body's brightest pixel was recorded in Excel. The frequency of a LacO position relative to the spindle pole was compiled for a single quadrant of the spindle and then mirrored about the spindle axis. The frequency of LacO position relative to the spindle pole was transferred to MATLAB to generate a 2D probability map using black body radiation spectrum (black represents zero probability, red and orange represent low probability, and yellow and white represent high probability). Heat maps were interpolated twice using this MATLAB code. The distance in pixels from the spindle pole body to the LacO in the x and y planes for each LacO was averaged to yield a distance from the spindle pole (x) and radial displacement from the spindle axis (y).

Strains

Strains used were as follows: KBY 8088 MATa ade1, met14, ura3-52, leu2-3,112 his3-11,15 lys2Δ::lacI-GFP-NLS-NAT, 1.1 kb CEN 3::LacO-KAN (1.2-kb array), Spc29RFP:Hb; KBY 8065 MATa ade2-1, his3-11, trp1-1, ura3-1, leu2-3,112 can1-100 LacINLSGFP:HIS3, LacO::URA3 (1.8 kb from CEN 15, 10-kb array) Spc29RFP:Hb; KBY 8087 MATa ade2-1, his3-11, trp1-1, ura3-1, leu2-3,112 can1-100 LacINLSGFP:HIS3, LacO::URA3 (3.8 kb from CEN 15, 10-kb array), Spc29CFP:Hb; KBY 8062 MATa ade2-1, his3-11, trp1-1, ura3-1, leu2-3,112 can1-100 LacINLSGFP:HIS3, LacO::URA3 (1.8 kb from CEN 15, 10-kb array) Spc29RFP:Hb, HHT1::TRP, KAN-GAL-HHT2; KBY 9039 MATa ade2-1, his3-11, trp1-1, ura3-1, leu2-3,112 can1-100 LacINLSGFP:HIS3, LacO::URA3 (1.8 kb from CEN 15, 10-kb array) Spc29RFP:Hb, *brn1-9*–Nat; KBY 9040 MATa ade2-1, his3-11, trp1-1, ura3-1, leu2-3,112 can1-100 LacINLSGFP:HIS3, LacO::URA3 (1.8 kb from CEN 15, 10-kb array) Spc29RFP:Hb, *mcd1-1;* KBY 9059 MATa ade2-1, his3-11, trp1-1, ura3-1, leu2-3,112 can1-100 LacINLSGFP:HIS3, LacO::URA3 (1.8 kb from CEN 15, 10-kb array) Spc29RFP:Hb, *mcm21*Δ::Nat; YSB 9025 (α) *smc4-1*, *ade2*, *ade3*Δ, *his3*, *leu2*, *trp-1*, Spc29-RFP:Hb, Nuf2-GFP-URA (S. Bachellier-Bassi, Institut Pasteur, Paris, France); YEF473 *MATa trp1-63 leu2Δ1 ura3-52*, *his2-200*, *lys2–801* (J. Pringle, Stanford University, Stanford, CA); KBY 9013 (473A) *mcd1-1*, Spc29-RFP-Hb, Nuf2-GFP-URA; MAY 8526 (YEF473A) Nuf2-GFP:Kan, Spc29-RFP-Hb; DCB 204 (YEF473A) HHT1::TRP1, KAN-GALp-HHT2, SPC29-RFP-Hb, NUF2-GFP-URA; KBY 9053 (YEF473A) *brn1-9*–NAT, Spc29-RFP-Hb, Nuf2-GFP-URA; KBY 9070 (YEF 473A) *mcm21*::Nat, Spc29-RFP-Hb, Nuf2-GFP-URA; WLY 8912 (YEF 473A) pLF639 (URA3 Smc3-GFP), Spc29-RFP-Hb; KBY 9035 (YEF 473A) Smc4-GFP-Kan, Spc29-RFP-Hb; KBY 9131 (YEF 473A) *brn1-9*–NAT, Spc29-RFP-Hb, Nuf2-GFP-URA, *kip1*Δ::HIS3; KBY 9122 (YEF 473A) *mcm21*::Nat, Spc29-RFP-Hb, Nuf2-GFP-URA, *kip1*Δ::HIS3; KBY 9117 (YEF 473A) *mcd1-1*, Spc29-RFP-Hb, Nuf2-GFP-URA, *kip1*Δ::HIS3; KBY 9357 (YEF 473A) pJB2#4 Spc29-RFP-Hb; and KBY 9169 (YEF 473A) gal2::HIS3, pGALS-CDC20-Nat, Spc29-RFP-Hb.

Plasmids

Plasmids used were pSO1 *brn1-9*–NAT (B. Lavoie, University of Toronto, Toronto, Ontario, Canada) and pLF639 (URA3 Smc3-GFP; A. Strunnikov, National Institutes of Health, Bethesda, MD).

Online supplemental material

Fig. S1 shows that the deletion of *MCM21* specifically decreases pericentric cohesin. Fig. S2 details interkinetochore and kinetochore microtubule length and variation. Fig. S3 shows that the dynamics of pericentric 6.8 kb LacO stretching correlate with spindle length changes. Table S1 lists the mean percentages for each class of pericentric LacO at 6.8 kb from CEN 15 fluorescence binned by spindle length. Online supplemental material is available at http://www.jcb.org/cgi/content/full/jcb.201103138/DC1.

We thank the reviewers for their critical and substantive comments. We thank A. Strunnikov for the Smc3-GFP plasmid, the B. Lavoie laboratory for the condensin temperature-sensitive plasmids, and the S. Bachellier-Bassi laboratory for *smc4-1* strains. We thank Guy vin Chang for work in imaging Smc3-GFP cohesin. We thank members of the Bloom laboratory for advice, assistance, and critical readings of the manuscript.

This work was funded by the National Institutes of Health R01 grant GM32238 (to K. Bloom).

Submitted: 25 March 2011
Accepted: 25 May 2011

References

Almagro, S., D. Riveline, T. Hirano, B. Houchmandzadeh, and S. Dimitrov. 2004. The mitotic chromosome is an assembly of rigid elastic axes organized by structural maintenance of chromosomes (SMC) proteins and surrounded by a soft chromatin envelope. *J. Biol. Chem.* 279:5118–5126. doi:10.1074/jbc.M307221200

Anderson, M., J. Haase, E. Yeh, and K. Bloom. 2009. Function and assembly of DNA looping, clustering, and microtubule attachment complexes within a eukaryotic kinetochore. *Mol. Biol. Cell*. 20:4131–4139. doi:10.1091/mbc.E09-05-0359

Bachant, J., A. Alcasabas, Y. Blat, N. Kleckner, and S.J. Elledge. 2002. The SUMO-1 isopeptidase Smt4 is linked to centromeric cohesion through SUMO-1 modification of DNA topoisomerase II. *Mol. Cell*. 9:1169–1182. doi:10.1016/S1097-2765(02)00543-9

Bachellier-Bassi, S., O. Gadal, G. Bourout, and U. Nehrbass. 2008. Cell cycle-dependent kinetochore localization of condensin complex in *Saccharomyces cerevisiae*. *J. Struct. Biol.* 162:248–259. doi:10.1016/j.jsb.2008.01.002

Bloom, K., and A. Joglekar. 2010. Towards building a chromosome segregation machine. *Nature*. 463:446–456. doi:10.1038/nature08912

Bouck, D.C., and K. Bloom. 2007. Pericentric chromatin is an elastic component of the mitotic spindle. *Curr. Biol.* 17:741–748. doi:10.1016/j.cub.2007.03.033

Bouck, D.C., A.P. Joglekar, and K.S. Bloom. 2008. Design features of a mitotic spindle: balancing tension and compression at a single microtubule kinetochore interface in budding yeast. *Annu. Rev. Genet.* 42:335–359. doi:10.1146/annurev.genet.42.110807.091620

Bustamante, C., J.F. Marko, E.D. Siggia, and S. Smith. 1994. Entropic elasticity of lambda-phage DNA. *Science*. 265:1599–1600. doi:10.1126/science.8079175

Cheeseman, I.M., and A. Desai. 2008. Molecular architecture of the kinetochore-microtubule interface. *Nat. Rev. Mol. Cell Biol.* 9:33–46. doi:10.1038/nrm2310

D'Ambrosio, C., C.K. Schmidt, Y. Katou, G. Kelly, T. Itoh, K. Shirahige, and F. Uhlmann. 2008. Identification of cis-acting sites for condensin loading onto budding yeast chromosomes. *Genes Dev.* 22:2215–2227. doi:10.1101/gad.1675708

Eckert, C.A., D.J. Gravdahl, and P.C. Megee. 2007. The enhancement of pericentromeric cohesin association by conserved kinetochore components promotes high-fidelity chromosome segregation and is sensitive to microtubule-based tension. *Genes Dev.* 21:278–291. doi:10.1101/gad.1498707

Finch, J.T., and A. Klug. 1976. Solenoidal model for superstructure in chromatin. *Proc. Natl. Acad. Sci. USA*. 73:1897–1901. doi:10.1073/pnas.73.6.1897

Fisher, J.K., M. Ballenger, E.T. O'Brien, J. Haase, R. Superfine, and K. Bloom. 2009. DNA relaxation dynamics as a probe for the intracellular environment. *Proc. Natl. Acad. Sci. USA*. 106:9250–9255. doi:10.1073/pnas.0812723106

Fitzgerald-Hayes, M., L. Clarke, and J. Carbon. 1982. Nucleotide sequence comparisons and functional analysis of yeast centromere DNAs. *Cell*. 29:235–244. doi:10.1016/0092-8674(82)90108-8

Gardner, M.K., C.G. Pearson, B.L. Sprague, T.R. Zarzar, K. Bloom, E.D. Salmon, and D.J. Odde. 2005. Tension-dependent regulation of microtubule dynamics at kinetochores can explain metaphase congression in yeast. *Mol. Biol. Cell*. 16:3764–3775. doi:10.1091/mbc.E05-04-0275

Gardner, M.K., J. Haase, K. Mythreye, J.N. Molk, M. Anderson, A.P. Joglekar, E.T. O'Toole, M. Winey, E.D. Salmon, D.J. Odde, and K. Bloom. 2008. The microtubule-based motor Kar3 and plus end–binding protein Bim1 provide structural support for the anaphase spindle. *J. Cell Biol.* 180:91–100. doi:10.1083/jcb.200710164

Glynn, E.F., P.C. Megee, H.G. Yu, C. Mistrot, E. Unal, D.E. Koshland, J.L. DeRisi, and J.L. Gerton. 2004. Genome-wide mapping of the cohesin complex in the yeast *Saccharomyces cerevisiae*. *PLoS Biol.* 2:E259. doi:10.1371/journal.pbio.0020259

Downloaded from jcb.rupress.org on December 22, 2011

Published June 27, 2011

Goshima, G., and M. Yanagida. 2000. Establishing biorientation occurs with precocious separation of the sister kinetochores, but not the arms, in the early spindle of budding yeast. *Cell*. 100:619–633. doi:10.1016/S0092-8674(00)80699-6

Grinthal, A., I. Adamovic, B. Weiner, M. Karplus, and N. Kleckner. 2010. PR65, the HEAT-repeat scaffold of phosphatase PP2A, is an elastic connector that links force and catalysis. *Proc. Natl. Acad. Sci. USA*. 107:2467–2472. doi:10.1073/pnas.0914073107

Grosberg, A.Y., and A.R. Khokhlov. 1997. Giant Molecules Here, There, and Everywhere. Academic Press, San Diego, CA. 244 pp.

Guacci, V., E. Hogan, and D. Koshland. 1994. Chromosome condensation and sister chromatid pairing in budding yeast. *J. Cell Biol.* 125:517–530. doi:10.1083/jcb.125.3.517

Guacci, V., D. Koshland, and A. Strunnikov. 1997. A direct link between sister chromatid cohesion and chromosome condensation revealed through the analysis of MCD1 in *S. cerevisiae*. *Cell*. 91:47–57. doi:10.1016/S0092-8674(01)80008-8

Guillou, E., A. Ibarra, V. Coulon, J. Casado-Vela, D. Rico, I. Casal, E. Schwob, A. Losada, and J. Méndez. 2010. Cohesin organizes chromatin loops at DNA replication factories. *Genes Dev.* 24:2812–2822. doi:10.1101/gad.608210

Hartwell, L.H., R.K. Mortimer, J. Culotti, and M. Culotti. 1973. Genetic control of the cell division cycle in yeast: V. genetic analysis of cdc mutants. *Genetics*. 74:267–286.

Heidinger-Pauli, J.M., O. Mert, C. Davenport, V. Guacci, and D. Koshland. 2010. Systematic reduction of cohesin differentially affects chromosome segregation, condensation, and DNA repair. *Curr. Biol.* 20:957–963. doi:10.1016/j.cub.2010.04.018

Hirano, T. 2006. At the heart of the chromosome: SMC proteins in action. *Nat. Rev. Mol. Cell Biol.* 7:311–322. doi:10.1038/nrm1909

Hou, C., R. Dale, and A. Dean. 2010. Cell type specificity of chromatin organization mediated by CTCF and cohesin. *Proc. Natl. Acad. Sci. USA*. 107:3651–3656. doi:10.1073/pnas.0912087107

Hu, B., T. Itoh, A. Mishra, Y. Katoh, K.L. Chan, W. Upcher, C. Godlee, M.B. Roig, K. Shirahige, and K. Nasmyth. 2011. ATP hydrolysis is required for relocating cohesin from sites occupied by its Scc2/4 loading complex. *Curr. Biol.* 21:12–24. doi:10.1016/j.cub.2010.12.004

Kagey, M.H., J.J. Newman, S. Bilodeau, Y. Zhan, D.A. Orlando, N.L. van Berkum, C.C. Ebmeier, J. Goossens, P.B. Rahl, S.S. Levine, et al. 2010. Mediator and cohesin connect gene expression and chromatin architecture. *Nature*. 467:430–435. doi:10.1038/nature09380

Kawamura, R., L.H. Pope, M.O. Christensen, M. Sun, K. Terekhova, F. Boege, C. Mielke, A.H. Andersen, and J.F. Marko. 2010. Mitotic chromosomes are constrained by topoisomerase II–sensitive DNA entanglements. *J. Cell Biol.* 188:653–663. doi:10.1083/jcb.200910085

Kimura, K., and T. Hirano. 1997. ATP-dependent positive supercoiling of DNA by 13S condensin: a biochemical implication for chromosome condensation. *Cell*. 90:625–634. doi:10.1016/S0092-8674(00)80524-3

Lam, W.W., E.A. Peterson, M. Yeung, and B.D. Lavoie. 2006. Condensin is required for chromosome arm cohesion during mitosis. *Genes Dev.* 20:2973–2984. doi:10.1101/gad.1468806

Lavoie, B.D., K.M. Tuffo, S. Oh, D. Koshland, and C. Holm. 2000. Mitotic chromosome condensation requires Brn1p, the yeast homologue of Barren. *Mol. Biol. Cell*. 11:1293–1304.

Lavoie, B.D., E. Hogan, and D. Koshland. 2002. In vivo dissection of the chromosome condensation machinery: reversibility of condensation distinguishes contributions of condensin and cohesin. *J. Cell Biol.* 156:805–815. doi:10.1083/jcb.200109056

Lavoie, B.D., E. Hogan, and D. Koshland. 2004. In vivo requirements for rDNA chromosome condensation reveal two cell-cycle-regulated pathways for mitotic chromosome folding. *Genes Dev.* 18:76–87. doi:10.1101/gad.1150404

Lengronne, A., Y. Katou, S. Mori, S. Yokobayashi, G.P. Kelly, T. Itoh, Y. Watanabe, K. Shirahige, and F. Uhlmann. 2004. Cohesin relocation from sites of chromosomal loading to places of convergent transcription. *Nature*. 430:573–578. doi:10.1038/nature02742

Manning, A.L., M.S. Longworth, and N.J. Dyson. 2010. Loss of pRB causes centromere dysfunction and chromosomal instability. *Genes Dev.* 24:1364–1376. doi:10.1101/gad.1917310

Megee, P.C., C. Mistrot, V. Guacci, and D. Koshland. 1999. The centromeric sister chromatid cohesion site directs Mcd1p binding to adjacent sequences. *Mol. Cell*. 4:445–450. doi:10.1016/S1097-2765(00)80347-0

Michaelis, C., R. Ciosk, and K. Nasmyth. 1997. Cohesins: chromosomal proteins that prevent premature separation of sister chromatids. *Cell*. 91:35–45. doi:10.1016/S0092-8674(01)80007-6

Mishiro, T., K. Ishihara, S. Hino, S. Tsutsumi, H. Aburatani, K. Shirahige, Y. Kinoshita, and M. Nakao. 2009. Architectural roles of multiple chromatin insulators at the human apolipoprotein gene cluster. *EMBO J.* 28:1234–1245. doi:10.1038/emboj.2009.81

Moore, L.L., G. Stanvitch, M.B. Roth, and D. Rosen. 2005. HCP-4/CENP-C promotes the prophase timing of centromere resolution by enabling the centromere association of HCP-6 in *Caenorhabditis elegans*. *Mol. Cell. Biol.* 25:2583–2592. doi:10.1128/MCB.25.7.2583-2592.2005

Nasmyth, K., and C.H. Haering. 2009. Cohesin: its roles and mechanisms. *Annu. Rev. Genet.* 43:525–558. doi:10.1146/annurev-genet-102108-134233

Nativio, R., K.S. Wendt, Y. Ito, J.E. Huddleston, S. Uribe-Lewis, K. Woodfine, C. Krueger, W. Reik, J.M. Peters, and A. Murrell. 2009. Cohesin is required for higher-order chromatin conformation at the imprinted IGF2-H19 locus. *PLoS Genet.* 5:e1000739. doi:10.1371/journal.pgen.1000739

Neuwald, A.F., and T. Hirano. 2000. HEAT repeats associated with condensins, cohesins, and other complexes involved in chromosome-related functions. *Genome Res.* 10:1445–1452. doi:10.1101/gr.147400

Ng, T.M., W.G. Waples, B.D. Lavoie, and S. Biggins. 2009. Pericentromeric sister chromatid cohesion promotes kinetochore biorientation. *Mol. Biol. Cell*. 20:3818–3827. doi:10.1091/mbc.E09-04-0330

Panizza, S., T. Tanaka, A. Hochwagen, F. Eisenhaber, and K. Nasmyth. 2000. Pds5 cooperates with cohesin in maintaining sister chromatid cohesion. *Curr. Biol.* 10:1557–1564. doi:10.1016/S0960-9822(00)00854-X

Pearson, C.G., P.S. Maddox, E.D. Salmon, and K. Bloom. 2001. Budding yeast chromosome structure and dynamics during mitosis. *J. Cell Biol.* 152:1255–1266. doi:10.1083/jcb.152.6.1255

Pearson, C.G., E. Yeh, M. Gardner, D. Odde, E.D. Salmon, and K. Bloom. 2004. Stable kinetochore-microtubule attachment constrains centromere positioning in metaphase. *Curr. Biol.* 14:1962–1967. doi:10.1016/j.cub.2004.09.086

Peters, J.P. III, and L.J. Maher. 2010. DNA curvature and flexibility in vitro and in vivo. *Q. Rev. Biophys.* 43:23–63. doi:10.1017/S0033583510000077

Ribeiro, S.A., J.C. Gatlin, Y. Dong, A. Joglekar, L. Cameron, D.F. Hudson, C.J. Farr, B.F. McEwen, E.D. Salmon, W.C. Earnshaw, and P. Vagnarelli. 2009. Condensin regulates the stiffness of vertebrate centromeres. *Mol. Biol. Cell*. 20:2371–2380. doi:10.1091/mbc.E08-11-1127

Sakuno, T., K. Tada, and Y. Watanabe. 2009. Kinetochore geometry defined by cohesion within the centromere. *Nature*. 458:852–858. doi:10.1038/nature07876

Samoshkin, A., A. Arnaoutov, L.E. Jansen, I. Ouspenski, L. Dye, T. Karpova, J. McNally, M. Dasso, D.W. Cleveland, and A. Strunnikov. 2009. Human condensin function is essential for centromeric chromatin assembly and proper sister kinetochore orientation. *PLoS ONE*. 4:e6831. doi:10.1371/journal.pone.0006831

Saunders, W.S., and M.A. Hoyt. 1992. Kinesin-related proteins required for structural integrity of the mitotic spindle. *Cell*. 70:451–458. doi:10.1016/0092-8674(92)90169-D

Straight, A.F., J.W. Sedat, and A.W. Murray. 1998. Time-lapse microscopy reveals unique roles for kinesins during anaphase in budding yeast. *J. Cell Biol.* 143:687–694. doi:10.1083/jcb.143.3.687

Strick, T.R., T. Kawaguchi, and T. Hirano. 2004. Real-time detection of single-molecule DNA compaction by condensin I. *Curr. Biol.* 14:874–880. doi:10.1016/j.cub.2004.04.038

Tanaka, T., M.P. Cosma, K. Wirth, and K. Nasmyth. 1999. Identification of cohesin association sites at centromeres and along chromosome arms. *Cell*. 98:847–858. doi:10.1016/S0092-8674(00)81518-4

Tanaka, T., J. Fuchs, J. Loidl, and K. Nasmyth. 2000. Cohesin ensures bipolar attachment of microtubules to sister centromeres and resists their precocious separation. *Nat. Cell Biol.* 2:492–499. doi:10.1038/35019529

Tremethick, D.J. 2007. Higher-order structures of chromatin: the elusive 30 nm fiber. *Cell*. 128:651–654. doi:10.1016/j.cell.2007.02.008

Uchida, K.S., K. Takagaki, K. Kumada, Y. Hirayama, T. Noda, and T. Hirota. 2009. Kinetochore stretching inactivates the spindle assembly checkpoint. *J. Cell Biol.* 184:383–390. doi:10.1083/jcb.200811028

Warsi, T.H., M.S. Navarro, and J. Bachant. 2008. DNA topoisomerase II is a determinant of the tensile properties of yeast centromeric chromatin and the tension checkpoint. *Mol. Biol. Cell*. 19:4421–4433. doi:10.1091/mbc.E08-05-0547

Weber, S.A., J.L. Gerton, J.E. Polancic, J.L. DeRisi, D. Koshland, and P.C. Megee. 2004. The kinetochore is an enhancer of pericentric cohesin binding. *PLoS Biol.* 2:E260. doi:10.1371/journal.pbio.0020260

Winey, M., C.L. Mamay, E.T. O'Toole, D.N. Mastronarde, T.H. Giddings Jr., K.L. McDonald, and J.R. McIntosh. 1995. Three-dimensional ultrastructural analysis of the *Saccharomyces cerevisiae* mitotic spindle. *J. Cell Biol.* 129:1601–1615. doi:10.1083/jcb.129.6.1601

Yang, S.S., E. Yeh, E.D. Salmon, and K. Bloom. 1997. Identification of a mid-anaphase checkpoint in budding yeast. *J. Cell Biol.* 136:345–354. doi:10.1083/jcb.136.2.345

Downloaded from jcb.rupress.org on December 22, 2011

Published June 27, 2011

Yeh, E., J. Haase, L.V. Paliulis, A. Joglekar, L. Bond, D. Bouck, E.D. Salmon, and K.S. Bloom. 2008. Pericentric chromatin is organized into an intramolecular loop in mitosis. *Curr. Biol.* 18:81–90. doi:10.1016/j.cub.2007.12.019

Yong-Gonzalez, V., B.D. Wang, P. Butylin, I. Ouspenski, and A. Strunnikov. 2007. Condensin function at centromere chromatin facilitates proper kinetochore tension and ensures correct mitotic segregation of sister chromatids. *Genes Cells*. 12:1075–1090. doi:10.1111/j.1365-2443.2007.01109.x

Yoshimura, S.H., K. Hizume, A. Murakami, T. Sutani, K. Takeyasu, and M. Yanagida. 2002. Condensin architecture and interaction with DNA: regulatory non-SMC subunits bind to the head of SMC heterodimer. *Curr. Biol.* 12:508–513. doi:10.1016/S0960-9822(02)00719-4

Downloaded from jcb.rupress.org on December 22, 2011